Optical Engineering

SPIEDigitalLibrary.org/oe

Finite element optical modeling of liquid crystal waveguides

Pieter J. M. Vanbrabant
Jeroen Beeckman
Kristiaan Neyts
Richard James
F. Anibal Fernandez

Finite element optical modeling of liquid crystal waveguides

Pieter J. M. Vanbrabant
Jeroen Beeckman
Kristiaan Neyts
Ghent University
Department of Electronics and Information Systems
B-9000 Ghent, Belgium
E-mail: Pieter.Vanbrabant@elis.ugent.be

Richard James
F. Anibal Fernandez
University College London
Electronic and Electrical Engineering Department
Torrington Place
London WC1E 7JE, United Kingdom

Abstract. A finite element modesolver and beam propagation (BPM) algorithm are applied to the optical analysis of liquid crystal waveguides. Both approaches are used in combination with advanced liquid crystal calculations and include a full dielectric tensor in solving the Helmholtz equation to model the liquid crystal behavior properly. Simulation of the beam propagation in a waveguide with tunable liquid crystal cladding layer illustrates the coupling of a Gaussian beam to the fundamental waveguide mode obtained with the modesolver. Excellent quantitative agreement between both approaches illustrates the potential of these methods for the design of advanced devices. The high accuracy of the BPM algorithm for wide angle propagation, essential in the analysis of high index contrast waveguides, is illustrated for angles up to 40 deg. © *2011 Society of Photo-Optical Instrumentation Engineers (SPIE).* [DOI: 10.1117/1.3564593]

Subject terms: liquid crystals; waveguides; modesolver; beam propagation method; finite element method.

Paper 100740SSR received Sep. 8, 2010; revised manuscript received Dec. 16, 2010; accepted for publication Dec. 21, 2010; published online Jun. 14, 2011.

1 Introduction

The breakthrough of liquid crystal devices during the past two decades is remarkable. Liquid crystal displays[1–3] have led to a new era in the mobile and display market segment because of their excellent performance in specifications such as power consumption, contrast ratio, viewing angle, and refresh rate. Furthermore, the electro-optic properties of liquid crystals have been widely applied to design tunable photonic components such as optical switches,[4] directional couplers,[5] ring resonators,[6] and filters.[7] The liquid crystal is typically used in these waveguide structures either as a tunable cladding material[8] or as the guiding material itself.[9–11]

Nematic liquid crystals (LCs)[12] are uniaxial mesophases that exhibit a long range orientational order in combination with a translational freedom of the molecules. The orientation of the liquid crystal can be controlled externally by electrical bias because of the dielectric anisotropy of the molecules which leads in combination with the optical uniaxiality to excellent electro-optical properties. It is essential to have a good understanding of the light propagation in advanced liquid crystal devices to keep their improvement ongoing. Optical modeling of such devices is however complicated because the optical tensor contains up to six different coefficients due to the inhomogeneous nature and optical anisotropy of the liquid crystal. This is often handled with some approximations in terms of the anisotropy or dimensionality.[13–16]

The finite element method has been applied for decades as a versatile numerical tool to obtain approximate solutions to boundary-value problems. Using a finite element scheme offers high accuracy in combination with the flexibility to model arbitrarily curved structures. Two rigorous finite element approaches for the optical analysis of waveguides with a liquid crystal cladding layer are applied and compared in this work. The most common approach in the design of waveguides is to analyze the electromagnetic modes supported by the structure. A finite element modesolver for anisotropic devices has been reported recently[17] to make this approach also applicable to waveguides with liquid crystal as the guiding material or cladding layer. Alternatively, the light propagation in waveguides can be simulated with a beam propagation method (BPM).[18–25] The BPM is an efficient and versatile numerical method that simulates the electric field propagation of a user-defined input optical field through arbitrary structures. The computational complexity of the method can be considered as optimal because the numerical effort is directly proportional to the number of mesh points used in the simulation.[21] Several finite element BPMs for LC devices have been described but the descriptions are either limited to transverse anisotropy[15,16] ($\epsilon_{zx} = \epsilon_{zy} = 0$) or paraxial propagation.[26] Recently, a full-vector wide angle finite element beam propagation method dedicated to the optical analysis of liquid crystal devices has been presented.[27]

In this paper, the modesolver and BPM are compared for the optical analysis of liquid crystal waveguides to illustrate the consistency of both methods and to show they are both attractive for modeling and designing LC waveguides. The basic principles of the finite element modesolver and BPM are reviewed in Sec. 2. The liquid crystal orientation is first calculated with an external solver[28] and the obtained director profile is considered in the optical analysis. The results obtained with both approaches are compared in Sec. 3.1. It is important to consider the wide angle properties of the BPM because they are essential to have an accurate description of the light propagation in high index contrast waveguides. Section 3.2 illustrates the propagation of a Gaussian beam in vacuum at various angles up to 40 deg with respect to the propagation direction z. The results are compared with the classical analytical description of Gaussian beams in homogeneous media to prove the high accuracy of the presented BPM algorithm for wide angle propagation.

2 Finite Element Modesolver and BPM for Liquid Crystal Devices

The inhomogeneous nature of the liquid crystal has to be taken into account when solving the Maxwell equations to calculate the light propagation or waveguide eigenmodes in LC devices accurately. Therefore, a full dielectric tensor has to be taken into account in the finite element discretization of the Helmholtz equation as presented in Sec 2.1. Next, the obtained wave equation can be applied for the calculation of waveguide eigenmodes or propagation analysis as described in Secs. 2.2 and 2.3, respectively.

2.1 *Finite Element Discretization of the Wave Equation*

The Helmholtz equation for the electric field $\mathbf{E}(x, y, z)$ is the starting point to consider time harmonic fields:

$$\nabla\times(\bar{\bar{\mu}}^{-1}\nabla\times\mathbf{E}) - k_0^2\bar{\bar{\epsilon}}\cdot\mathbf{E} = 0, \tag{1}$$

where k_0 is the wavenumber in vacuum, $\bar{\bar{\epsilon}}$ is the relative permittivity tensor, and $\bar{\bar{\mu}}$ is the relative permeability tensor. A slowly varying envelope approximation is assumed to separate the electric field $\mathbf{E}$ into a slowly varying complex field $\mathbf{\Phi}(x, y, z) = \phi_x(x, y, z)\mathbf{1}_x + \phi_y(x, y, z)\mathbf{1}_y + \phi_z(x, y, z)\mathbf{1}_z$ and a phase factor $\exp(-jk_0n_0z)$, where z is the propagation direction:

$$\mathbf{E}(x, y, z) = \mathbf{\Phi}(x, y, z)\exp(-jk_0n_0z), \tag{2}$$

with n_0 an appropriate reference refractive index (see Sec. 3.1). Equation (1) is discretized in the finite element method by dividing the structure cross section Ω into small finite vector elements.[29] Such hybrid edge/nodal elements have been successfully applied in the modeling of vector fields in electromagnetism and optics because spurious solutions are excluded while the desired continuity conditions at dielectric interfaces are incorporated. The transverse and longitudinal field components are expanded within each element as:

$$\begin{bmatrix}\phi_x\\ \phi_y\\ \phi_z\end{bmatrix} = \begin{bmatrix}N_x^T & 0\\ N_y^T & 0\\ 0 & jL^T\end{bmatrix}\begin{bmatrix}\phi_t^e\\ \phi_z^e\end{bmatrix}, \tag{3}$$

where ϕ_t^e and ϕ_z^e are the edge and nodal values, respectively, in the element being considered. Hybrid LT/QN elements that use combined linear/quadratic tangential N_x and N_y and quadratic normal (QN) L shape functions for interpolation of the transverse and longitudinal field,[29] are applied. The LT/QN shape functions are preferred over first order functions for their higher-order convergence. The full dielectric permittivity tensor $\bar{\bar{\epsilon}}$ is maintained to model general anisotropic dielectric materials and a Galerkin procedure[30] is applied to the wave equation from Eq. (1). Substituting Eqs. (2) and (3) into Eq. (1) yields the basic equation for finite element optical analysis:

$$\begin{bmatrix}B_{tt} & 0\\ 0 & 0\end{bmatrix}\frac{\partial^2}{\partial z^2}\begin{bmatrix}\phi_t\\ \phi_z\end{bmatrix} - \begin{bmatrix}2jk_0n_0B_{tt} & jB_{tz}\\ jB_{zt} & 0\end{bmatrix}\frac{\partial}{\partial z}\begin{bmatrix}\phi_t\\ \phi_z\end{bmatrix} - \begin{bmatrix}A_{tt}+k_0^2n_0^2B_{tt} & -jC_{tz}+k_0n_0B_{tz}\\ jC_{zt}+k_0n_0B_{zt} & B_{zz}\end{bmatrix}\begin{bmatrix}\phi_t\\ \phi_z\end{bmatrix} = 0. \tag{4}$$

The submatrices in Eq. (4) can be calculated for general anisotropic dielectric materials according to the expressions in Ref. 27 if the variation $\partial\epsilon_{ii}/\partial z$ is sufficiently small. It is possible to derive a finite element modesolver and beam propagation algorithm based on Eq. (4) as described in Secs. 2.2 and 2.3, respectively.

2.2 *Modesolver Algorithm*

The waveguide eigenmodes can be calculated by assuming steady-state fields in Eq. (4) and rearranging the resulting expression as an eigenvalue problem. The numerical accuracy of the eigenvalue calculation can be improved by changing the finite element expansion in Eq. (3) to have edge and nodal values with comparable magnitudes. This can be achieved by multiplying the finite element expansion of the longitudinal field component in Eq. (3) with a factor $k_z = k_0n_0$ (according to the divergence relation $\nabla\cdot\bar{\bar{\epsilon}}\cdot\mathbf{E}$=0), yielding $\phi_z = jk_z[L]^T\phi_z^e$. As a result, the eigenvalue system changes to the following quadratic problem:[17]

$$\left\{k_z^2\begin{bmatrix}B_{tt} & B_{tz}\\ B_{zt} & B_{zz}\end{bmatrix} + k_z\begin{bmatrix}0 & jC_{tz}\\ -jC_{tz} & 0\end{bmatrix} - \begin{bmatrix}A_{tt} & 0\\ 0 & 0\end{bmatrix}\right\} \times\begin{bmatrix}\phi_t\\ \phi_z\end{bmatrix} = 0, \tag{5}$$

which reduces to a linear eigenvalue problem in the absence of dielectric anisotropy in the longitudinal direction (i.e., $\epsilon_{zx} = \epsilon_{zy} = 0$). The quadratic eigenvalue problem from Eq. (5) can be reduced in the general case to a linear system by doubling the number of unknowns.[31]

2.3 *Wide Angle Beam Propagation Algorithm*

The beam propagation method is used to calculate the evolution of time harmonic fields upon propagation. As described in, Ref. 27, it is possible to derive a recurrence scheme for the transverse field by eliminating ϕ_z from the second row of Eq. (4) and substituting the result into the first row of this equation. The resulting expression can be formally rewritten as a first order differential equation for the transverse field component:

$$\begin{bmatrix}A_{11} & A_{12}\\ I & 0\end{bmatrix}\frac{\partial}{\partial z}\begin{bmatrix}\phi_t\\ \frac{\partial\phi_t}{\partial z}\end{bmatrix} + \begin{bmatrix}B_{11} & 0\\ 0 & -I\end{bmatrix}\begin{bmatrix}\phi_t\\ \frac{\partial\phi_t}{\partial z}\end{bmatrix} = 0, \tag{6}$$

where I is the identity matrix of the same dimensions as the submatrices A_{11}, A_{12}, and B_{11} which are defined as:

$$A_{11} = -2jk_0n_0B_{tt} - B_{tz}B_{zz}^{-1}(C_{zt} - jk_0n_0B_{zt}) + (C_{tz} + jk_0n_0B_{tz})B_{zz}^{-1}B_{zt}, \tag{7}$$

$$A_{12} = B_{tt} - B_{tz}B_{zz}^{-1}B_{zt}, \tag{8}$$

$$B_{11} = (k_0n_0B_{tz} - jC_{tz})B_{zz}^{-1}(jC_{zt} + k_0n_0B_{zt}) - A_{tt} - k_0^2n_0^2B_{tt}. \tag{9}$$

Discretizing the derivative in Eq. (6) yields a recurrence scheme to propagate the transverse field in the z-direction:

$$Y_i\begin{bmatrix}\phi_t\\ \frac{\partial\phi_t}{\partial z}\end{bmatrix}_{i+1} = Z_i\begin{bmatrix}\phi_t\\ \frac{\partial\phi_t}{\partial z}\end{bmatrix}_i \tag{10}$$

with i the iteration number and

$$Y_i = \begin{bmatrix} A_{11} & A_{12} \\ I & 0 \end{bmatrix}_i + \vartheta \Delta z \begin{bmatrix} B_{11} & 0 \\ 0 & -I \end{bmatrix}_i, \tag{11}$$

$$Z_i = \begin{bmatrix} A_{11} & A_{12} \\ I & 0 \end{bmatrix}_i - (1-\vartheta)\Delta z \begin{bmatrix} B_{11} & 0 \\ 0 & -I \end{bmatrix}_i, \tag{12}$$

where Δz is the propagation step and ϑ is a parameter that controls the stability of the scheme. The subscript i for the system matrices Y and Z in Eq. (10) can be omitted for structures with a cross section that is invariant in the z-direction (e.g., waveguides). The evolution of the electric field upon wide angle propagation of the input optical field through the structure of interest can be calculated from the transverse field and its derivative at $z = 0$ by iteratively applying Eq. (10). This efficient scheme yields the transverse field ϕ_t and its derivative with respect to z in subsequent planes separated by Δz and the longitudinal field component ϕ_z is calculated from the transverse field. Furthermore, the approach automatically includes the effects of radiating fields as well as mode coupling and conversion.

2.4 *Implementation*

The modesolver and BPM have been implemented in MATLAB and take advantage of the efficient sparse matrix operations. Free versions of both methods can be downloaded from http://www.elis.ugent.be/ELISgroups/lcd/research/research.php. Calculating the waveguide eigenmodes for a mesh consisting of 5000 LT/QN elements typically takes about 300 s on a 2.5 GHz Intel Core 2 Duo CPU. The total calculation time to simulate light propagation with the BPM over, e.g., 100 μm in liquid crystal devices for a mesh consisting of 500 LT/QN elements takes about 400 s on the same computer. Perfectly matched layers (PML) for anisotropic media[32] are applied in the BPM for reflectionless absorption of electromagnetic waves at the borders of the computational window. Typically, the stability parameter is $\vartheta = 1$ and the propagation step is chosen equal to the light wavelength.

3 Applications and Accuracy Analysis

The modesolver and BPM are applied in Sec. 3.1 for the optical analysis of a waveguide with a liquid crystal cladding layer and the obtained results are compared to check their consistency. The liquid crystal orientation is first calculated with an external finite element solver[28] and the obtained director profile is considered in the optical simulations. Such compatibility is an important advantage of the presented finite element approach to realize accurate device modeling.

It is essential to prove that wide angle light propagation is correctly described in the BPM to show that the method is well-suited for accurate modeling of the light propagation in high index contrast waveguides. Therefore, the propagation of a Gaussian beam in vacuum at various angles up to 40 deg with respect to the propagation direction z is illustrated in Sec. 3.2. The results are compared with the classical analytical description of Gaussian beams in homogeneous media to prove the wide angle propagation properties of the presented BPM algorithm.

3.1 *Waveguide with a Liquid Crystal Cladding Layer*

A square strip waveguide of 1 μm × 1 μm with refractive index $n_1 = 1.65$ (e.g., a high index polymer) is considered on a glass substrate with $n_3 = 1.5$ as sketched in Fig. 1. The cladding layer is a 5-μm thick liquid crystal slab with ordinary and extraordinary refractive indices $n_{2,o} = 1.475$ and $n_{2,e} = 1.577$, respectively. The orientation of the liquid crystal can be controlled by applying a voltage between the two electrodes $E1$ and $E2$ indicated in Fig. 1 because of the dielectric anisotropy. A homogeneous orientation of the liquid crystal slab in the 0 V state can be realized by using an appropriate alignment layer[33] at the interfaces between this layer and the surrounding media. In this example, the liquid crystal has an initial planar alignment oriented along the z-axis with a 2 degree pretilt. Calculating the director profile in a liquid crystal device involves minimizing the total energy F (which comprises terms related to elastic, electric, and surface energy) while satisfying the boundary conditions (applied voltage and director orientation at the interfaces). To include variable order effects in calculations, a generalization of the theory on the free energy in liquid crystals has been described by Landau and de Gennes.[34] Instead of using a vector, the liquid crystal orientation is described by a tensor $\overline{\overline{Q}}$

$$\overline{\overline{Q}} = \frac{S_1}{2}(3\overline{L} \otimes \overline{L} - I) + \frac{S_2}{2}(3\overline{m} \otimes \overline{m} - I), \tag{13}$$

where $\otimes$ is the tensor product, I is the identity matrix, and S_1, respectively S_2 represent the order along the director $\overline{L}$ and a perpendicular unit vector $\overline{m}$. In addition to the elastic, electric and surface free energy densities and also a bulk free energy density f_{bulk} is included. The bulk free energy is a function of the order parameter and describes the phase of the material: uniaxial/biaxial nematic or isotropic. To calculate the swithing behavior of the liquid crystal, the free energy is supplemented by a dissipation term D to account for the dissipation of kinetic energy due to viscous forces. The variation of the director in time is calculated according to a dissipation principle:

$$\frac{\partial}{\partial \alpha}\frac{\partial F}{\partial \overline{\overline{Q}}_{,\alpha}} - \frac{\partial F}{\partial \overline{\overline{Q}}} - \frac{\partial D}{\partial \dot{\overline{\overline{Q}}}} = 0. \tag{14}$$

A two-dimensional finite element implementation described in Ref. 28 is used here to solve Eq. (14) with a time stepping

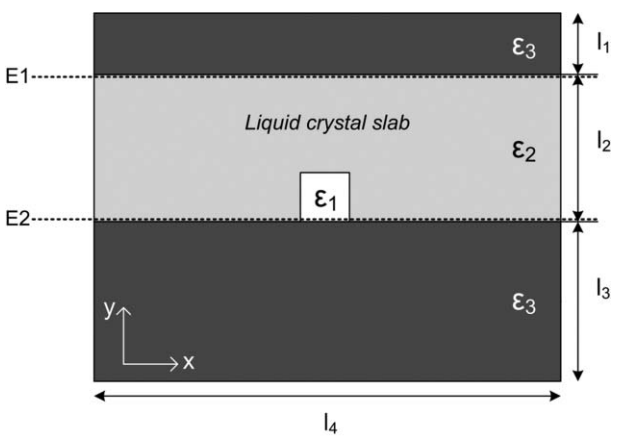

Fig. 1 Transverse cross section of the waveguide with a liquid crystal cladding layer.

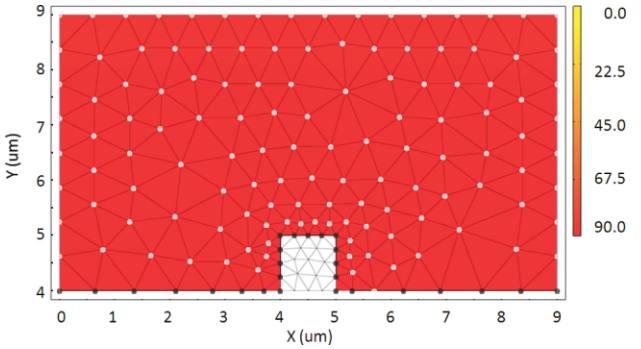

Fig. 2 Director profile of the liquid crystal cladding layer when 0 V is applied. The tilt θ of the director (the angle between the director and the y-axis) is indicated in the color bar.

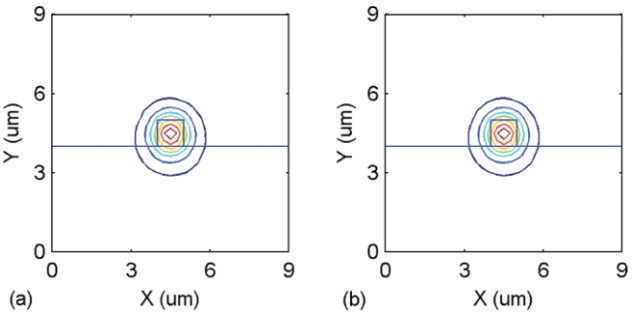

Fig. 4 The E_y field component after propagation over (a) 25 μm and (b) 75 μm in the waveguide when no voltage is applied. The contour plots are normalized to have equal maximum values for each frame.

approach. The Q-tensor is calculated at t_0 and the corresponding free energy F of the configuration is evaluated. Next, the time derivative of the Q-tensor $\dot{\overline{\overline{Q}}}$ is calculated and the dissipation D is evaluated. The values of $\{\overline{\overline{Q}}, \dot{\overline{\overline{Q}}}, D, F\}$ are updated in Eq. (14) and the procedure is repeated. In this way, the dynamic behavior of the liquid crystal in time is obtained.

Figures 2 and 3 show the obtained director profiles when 0 V and 7 V, respectively, are applied across the liquid crystal slab. It is clear from Fig. 3 that applying 7 V is sufficient to change the original planar alignment of the liquid crystal (Fig. 2) to a nearly vertical orientation. Changing the orientation of the liquid crystal alters the optical properties of the cladding layer because of its optical anisotropy.

The propagation of an input optical field $[0, E_y, E_z]$ with a vertical linear polarization and wavelength $\lambda = 1.5$ μm is simulated with the BPM to assess the optical properties of the waveguide with tunable cladding layer. The E_y field component has a Gaussian intensity profile centered in the waveguide. The computational window shown in Fig. 1 with dimensions $l_1 = 3$ μm, $l_2 = 5$ μm, $l_3 = 4$ μm, and $l_4 = 9$ μm is divided into 430 triangular finite elements and the propagation step is $\Delta z = 1$ μm. Figures 4 and 5 show the obtained evolution of the E_y component upon propagation along the waveguide for the 0 and 7 V situation.

Upon propagation, the original Gaussian field profile couples to the fundamental mode supported by the waveguide which is single-mode for $\lambda = 1.5$ μm. It is interesting to compare the evolution of the optical field in Figs. 4 and 5 to the waveguide modes calculated with the modesolver for anisotropic waveguides. Figures 6 and 7 show the TM mode profiles obtained for the 0 and 7 V director profiles. The effective indices of the modes are calculated as $n_{\text{eff},0\text{ V}} = 1.5603$ and $n_{\text{eff},7\text{ V}} = 1.5710$, respectively. As shown in Fig. 6, the mode is confined in the waveguide when no voltage is applied because of the high index contrast $\Delta n = n_1 - n_{2,o}$ between the core and the cladding layer. This index contrast is reduced to $\Delta n \approx n_1 - n_{2,e}$ for the 7 V case for vertically polarized light because of the near-vertical orientation of the liquid crystal. Therefore, the optical power is less confined as observed in Fig. 7. Comparing the simulated mode profiles from Figs. 6 and 7(a) to the optical fields obtained after beam propagation over $d \geq 75$ μm [Figs. 4(b) and 5(d)] reveals good qualitative agreement. As expected, the original Gaussian beam is clearly converted to the waveguide mode upon propagation.

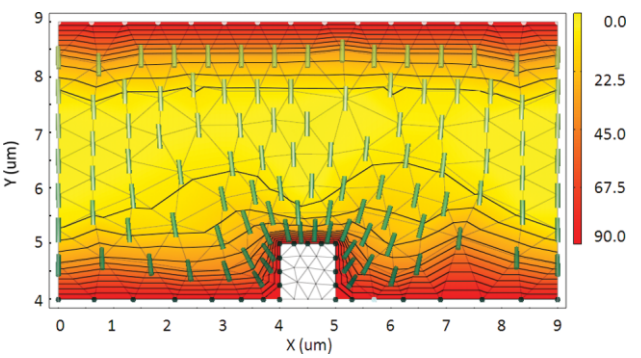

Fig. 3 Director profile of the liquid crystal cladding layer when 7 V is applied. The tilt θ of the director (the angle between the director and the y-axis) is indicated in the color bar.

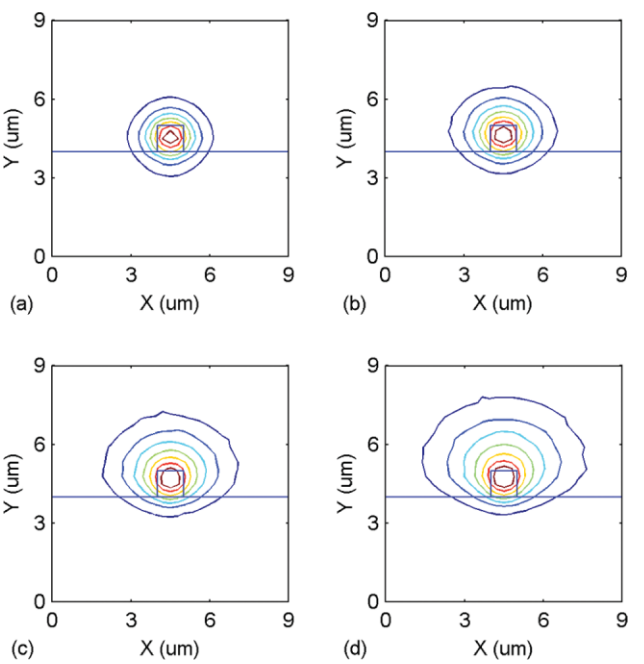

Fig. 5 The E_y field component after propagation over (a) 25 μm, (b) 50 μm, (c) 75 μm, and (d) 100 μm in the waveguide when 7 V is applied. The contour plots are normalized to have equal maximum values for each frame.

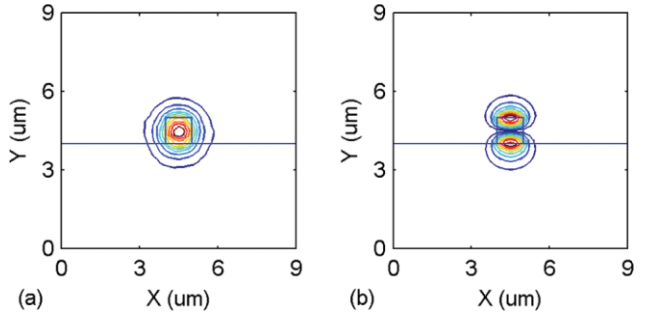

Fig. 6 TM mode profile when 0 V is applied: (a) E_y and (b) E_z.

The agreement between both approaches can be assessed in a quantitative way by comparing the evolution of the reference index n_0 upon propagation to the effective indices n_{eff} of the calculated waveguide modes. This reference index n_0 is renewed for every iteration step i as follows:[15]

$$n_{0,i} = \frac{1}{k_0}\text{Re}\left[\frac{-b_i + \sqrt{b_i^2 - 4a_i c_i}}{2a_i}\right] \tag{15}$$

with

$$a_i = \{\phi\}_i^\dagger \begin{bmatrix} B_{tt} & 0 \\ 0 & 0 \end{bmatrix} \{\phi\}_i, \tag{16}$$

$$b_i = \{\phi\}_i^\dagger \begin{bmatrix} 0 & B_{tz} \\ B_{zt} & 0 \end{bmatrix} \{\phi\}_i, \tag{17}$$

$$c_i = \{\phi\}_i^\dagger \begin{bmatrix} A_{tt} & -jC_{tz} \\ jC_{zt} & B_{zz} \end{bmatrix} \{\phi\}_i \tag{18}$$

where † denotes a Hermitian transpose. The expression for $n_{0,i}$ is obtained by solving the quadratic equation which is obtained by setting $\partial\phi_t/\partial z = 0$ and $\partial\phi_z/\partial z = 0$ in Eq. (4). Therefore, it follows that the value of $n_{0,i}$ according to Eq. (15) converges for waveguide modes to the effective index n_{eff}. Figures 8 and 9 show the evolution of n_0 upon propagation for the 0 V and 7 V case. In these simulations, PMLs are applied in the BPM for reflectionless absorption of the light which is not coupled to the waveguide mode. This mainly occurs at the beginning of the beam propagation when the Gaussian beam is converting to the waveguide mode. Once the mode is obtained, the light is trapped in the waveguide and there is no radiation toward the edges of

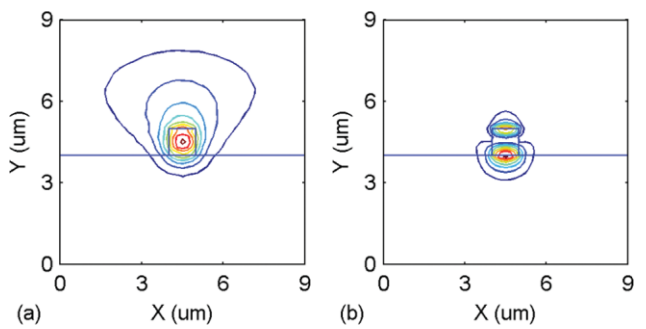

Fig. 7 TM mode profile when 7 V is applied: (a) E_y and (b) E_z.

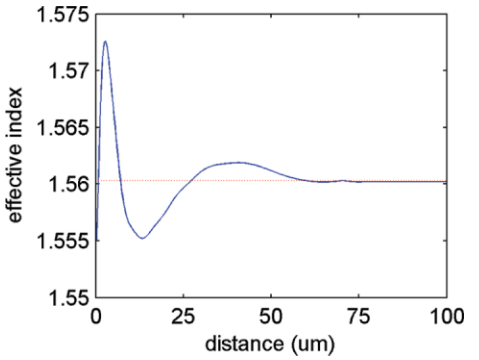

Fig. 8 Evolution of the reference index n_0 upon propagation when no voltage is applied. The dashed line indicates the calculated effective index $n_{\text{eff},0\text{ V}} = 1.5603$ of the waveguide mode.

the computational window. In this case, the influence of the PMLs on the value of n_0 is negligible. This is confirmed by the observation that the imaginary part of n_0 becomes zero while its real part converges for both cases to the obtained effective mode indices $n_{\text{eff},0\text{ V}}$ respectively $n_{\text{eff},7\text{ V}}$. This proves the conversion of the original field profiles to the waveguide modes. This excellent quantitative agreement illustrates the numerical accuracy of the presented methods. Because the waveguide mode is more similar to the original Gaussian field when no voltage is applied [Fig. 6(a)], the input beam converges faster for the 0 V case than for the 7 V case. This is confirmed in both the simulated profiles (Figs. 4 and 5) and the evolution of the reference index n_0 (Figs. 8 and 9).

As shown in this example, the BPM and modesolver are well-suited for the optical analysis of liquid crystal waveguides and the results obtained with both approaches are in good quantitative agreement. The modesolver approach might be preferred in designing waveguides because only a single eigenvalue problem has to be solved to obtain the updated effective mode indices after changing the structure. However, the BPM can be more closely related to experiments because the actual light propagation is calculated. This allows us to model the light coupling from a surrounding medium into a waveguide or to describe, e.g., the influence of the beam shape on the propagation characteristics.

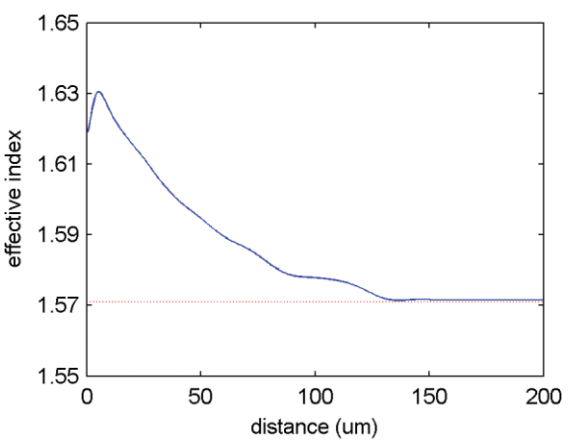

Fig. 9 Evolution of the reference index n_0 upon propagation for the 7 V case. The dashed line indicates the calculated effective index $n_{\text{eff},7\text{ V}} = 1.5710$ of the waveguide mode.

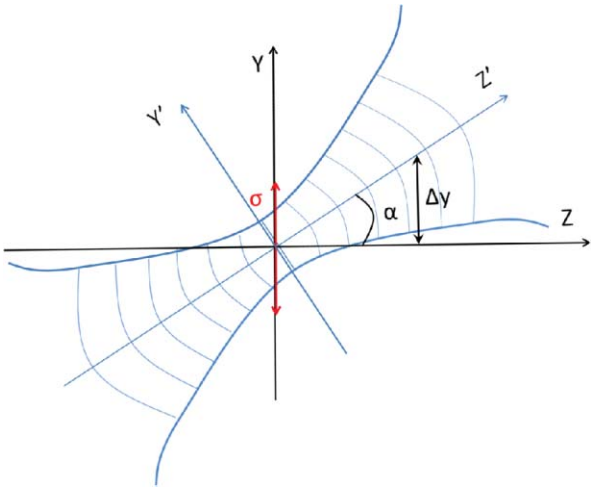

Fig. 10 Gaussian beam propagating at an angle α with respect to the z-axis.

3.2 *Gaussian Beam Propagation at Wide Angles in Vacuum*

An assessment of the BPM accuracy for wide angle propagation can be made by considering a Gaussian beam propagating at an angle α with respect to the z-axis. The electric field of the fundamental Gaussian beam solution to the wave equation in vacuum in a $x'y'z'$ coordinate system is well-known in optics:

$$E(x', y', z') \propto \frac{\omega_0}{\omega(z')} \exp[-j(k_0 z' - \eta(z'))] \times \exp\left[-(x'^2 + y'^2)\left(\frac{1}{\omega^2(z')} + \frac{jk_0}{2R(z')}\right)\right] \tag{19}$$

with the well-known expressions for the wavenumber k_0, the radius of curvature $R(z')$, the longitudinal phase delay $\eta(z')$, the spot size $\omega(z')$, and the beam waist ω_0.[35] The electric field of the Gaussian beam with wavelength $\lambda = 1\ \mu$m is calculated from Eq. (19) in a plane σ through the origin with the z-axis as normal as shown in Fig. 10. The beam is centered in the origin of a mesh which extends from $-5\omega_0$ to $5\omega_0$ in the X direction and from $-5\omega_0$ to $15\omega_0$ along Y where $\omega_0 = 1\ \mu$m is the beam waist of the beam. The edges of the elements are approximately equal to half the wavelength λ and the mesh contains about 1700 elements. The obtained field is discretized to a set of nodal and edge values and the recurrence scheme from Eq. (10) is applied with $\Delta z = 1\ \mu$m to calculate the evolution of the electric field in subsequent planes perpendicular to the z-direction. Obviously, the beam center will undergo a vertical translation $\Delta y = d\ \tan\alpha$ in these planes with d the propagation distance. Figure 11 shows the simulated vertical displacement Δy of the beam center (peak intensity) after propagation over $d = 5\ \mu$m in the z-direction as a function of the angle α. Comparing the simulated translation of the beam center with the theoretical translation Δy in Fig. 11 shows that the presented beam propagation algorithm offers high accuracy to model wide angle propagation up to 40 deg. Although a small numerical error for wide angles is inevitable because of the discretization of the derivative in Eq. (6), the method offers high accuracy because no first order approximations of the second order derivatives have been made in deriving the recurrence scheme from Eq. (4).

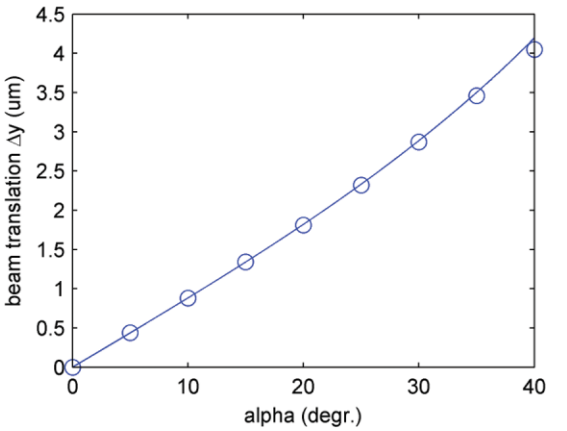

Fig. 11 Theoretical (solid) and simulated (circle) translation Δy of the beam center as a function of the angle α with respect to the z-axis.

4 Conclusions

A finite element modesolver and BPM algorithm for the optical analysis of liquid crystal waveguides have been compared. Both full-vector methods are compatible with advanced liquid crystal calculations and benefit from the flexibility to model arbitrary geometries. Furthermore, the approaches include a full dielectric tensor in solving the Helmholtz equation for the electric field to model the inhomogeneous and anisotropic nature of the liquid crystal properly. Simulation of the beam propagation in the waveguide with tunable liquid crystal cladding layer illustrates the coupling of a Gaussian beam to the fundamental waveguide mode obtained with the modesolver. The excellent quantitative agreement between both approaches illustrates the potential of these methods for the design of advanced devices. The high accuracy of the BPM algorithm for wide angle propagation, essential for the analysis of high index contrast waveguides, is illustrated by comparing the Gaussian beam propagation in vacuum at angles up to 40 deg with the classical analytical description.

Acknowledgments

Pieter J. M. Vanbrabant is a PhD Fellow of the Research Foundation Flanders (FWO) and Jeroen Beeckman is a Postdoctoral Fellow of the same institution. The work was carried out in the framework of the Interuniversity Attraction Poles program of the Belgian Science Policy Office, under grant IAP P6-10 "photonics@be."

1. H. Kawamoto, "The history of liquid-crystal displays," *Proc. IEEE* **90**, 460 (2002).
2. M. F. Schiekel and K. Fahrenschon, "Deformation of nematic liquid crystals with vertical orientation in electric fields," *Appl. Phys. Lett.* **19**, 391 (1971).
3. P. J. M. Vanbrabant, N. Dessaud, and J. F. Strömer, "Temperature influence on the dynamics of vertically aligned liquid crystal displays," *Appl. Phys. Lett.* **92**, 091101 (2008).
4. M. Kobayashi, H. Terui, M. Kawachi, and J. Noda, "2x2 optical-waveguide matrix switch using nematic liquid-crystal," *IEEE J. Quantum Electron.* **18**, 1603 (1982).
5. R. P. Pan, S. R. Liou, and C. K. Lin, "Voltage-controlled optical fiber coupler using a layer of low-refractive-index liquid crystal with positive dielectric anisotropy," *Jpn. J. Appl. Phys. Part 1* **34**, 6410 (1995).

6. W. De Cort, J. Beeckman, R. James, F. A. Fernandez, R. Baets, and K. Neyts, "Tuning of silicon-on-insulator ring resonator with liquid crystal cladding using the longitudinal field component," *Opt. Lett.* **34**, 2054 (2009).
7. J. S. Patel, M. A. Saifi, D. W. Berreman, C. L. Lin, N. Andreadakis, and S. D. Lee, "Electrically tunable optical filter for infrared wavelength using liquid-crystals in a fabry-perot etalon," *Appl. Phys. Lett.* **57**, 1718 (1990).
8. H. Desmet, W. Bogaerts, A. Adamski, J. Beeckman, K. Neyts, and R. Baets, "Silicon - on - insulator optical waveguides with liquid crystal cladding for switching and tuning," *Proc. ECOC* **3**, 430 (2003).
9. J. Beeckman, K. Neyts, X. Hutsebaut, C. Cambournac, and M. Haelterman, "Simulations and experiments on self-focusing conditions in nematic liquid-crystal planar cells," *Opt. Express* **12**, 1011 (2004).
10. A. d'Alessandro, B. Bellini, D. Donisi, R. Beccherelli, and R. Asquini, "Nematic liquid crystal optical channel waveguides on silicon," *IEEE J. Quantum Electron.* **42**, 1084 (2006).
11. J. Beeckman, K. Neyts, and M. Haelterman, "Patterned electrode steering of nematicons," *J. Opt. A: Pure Appl. Opt.* **8**, 214 (2006).
12. S. Chandrasekhar, *Liquid Crystals*, 2nd ed. Cambridge University Press, Cambridge, UK (1992).
13. R. Asquini and A. d'Alessandro, "Bpm analysis of an integrated optical switch using polymeric optical waveguides and ssflc at 1.55 um," *Mol. Cryst. Liq. Cryst.* **375**, 243 (2002).
14. G. Ntogari, D. Tsipouridou, and E. Kriezis, "A numerical study of optical switches and modulators based on ferroelectric liquid crystals," *J. Opt. A: Pure Appl. Opt.* **7**, 82 (2005).
15. K. Saitoh and M. Koshiba, "Full-vectorial finite element beam propagation method with perfectly matched layers for anisotropic optical waveguides," *J. Lightwave Technol.* **19**, 405 (2001).
16. D. Schulz, C. Glingener, M. Bludszuweit, and E. Voges, "Mixed finite element beam propagation method," *J. Lightwave Technol.* **16**, 1336 (1998).
17. J. Beeckman, R. James, F. A. Fernandez, W. De Cort, P. J. M. Vanbrabant, and K. Neyts, "Calculation of fully anisotropic liquid crystal waveguide modes," *J. Lightwave Technol.* **27**, 3812 (2009).
18. J. VanRoey, J. van der Donk, and P. E. Lagasse, "Beam-propagation method: Analysis and assessment," *J. Opt. Soc. Am.* **71**, 803 (1980).
19. M. Koshiba and K. Inoue, "Simple and efficient finite-element analysis of microwave and optical waveguides," *IEEE Trans. Microwave Theory Tech.* **40**, 371–377 (1992).
20. Y. Tsuji, M. Koshiba, and N. Takimoto, "Finite element beam propagation method for anisotropic optical waveguides," *J. Lightwave Techvol.*, **17**, 723 (1999).
21. R. Scarmozzino, A. Gopinath, R. Pregla, and S. Helfert, "Numerical techniques for modeling guided-wave photonic devices," *IEEE J. Sel. Top. Quant.* **6**, 150 (2000).
22. C. Ma and E. Van Keuren, "A three-dimensional wide-angle bpm for optical waveguide structures," *Opt. Express* **15**, 402 (2007).
23. C. Ma and E. Van Keuren, "A three-dimensional wide-angle bpm for optical waveguide structures," *Opt. Express* **15**, 402 (2007).
24. B. M. A. Rahman, D. M. H. Leung, S. S. A. Obbayya, and K. T. V. Grattan, "Numerical analysis of bent waveguides: Bending loss, transmission loss, mode coupling, and polarization coupling," *Appl. Opti.* **47**, 2961 (2008).
25. K. Q. Le and P. Bienstman, "Wide-angle beam propagation method without using slowly varying envelope approximation," *J. Opt. Soc. Am. B* **26**, 353 (2009).
26. G. D. Ziogos and E. E. Kriezis, "Modeling light propagation in liquid crystal devices with a 3-d full-vector finite-element beam propagation method," *Opt. Quantum Electron.* **40**, 733 (2008).
27. P. J. M. Vanbrabant, J. Beeckman, K. Neyts, R. James, and F. A. Fernandez, "A finite element beam propagation method for simulation of liquid crystal devices," *Opt. Express* **17**, 10895 (2009).
28. R. James, E. Willman, F. A. Fernandez, and S. E. Day, "Finite-element modeling of liquid-crystal hydrodynamics with a variable degree of order," *IEEE Trans. Electron. Dev.* **53**, 1575 (2006).
29. M. Koshiba and Y. Tsuji, "Curvilinear hybrid edge/nodal elements with triangular shape for guided-wave problems," *J. Lightwave Technol.* **18**, 737 (2000).
30. Jianming Jin, *The Finite Element Method in Electromagnetics*, Wiley New York, (2002).
31. F. Tisseur and K. Meerbergen, "The quadratic eigenvalue problem," *SIAM Rev.* **43**, 235 (2001).
32. F. L. Teixeira and W. C. Chew, "General closed-form pml constitutive tensors to match arbitrary bianisotropic and dispersive linear media," *IEEE Microw. Guid. Wave Lett.* **8**, 223 (1998).
33. P. J. M. Vanbrabant, J. Beeckman, and K. Neyts, "Tunable quasi-homeotropic liquid crystal pretilt angle based on competing alignment layers," *Liq. Cryst.* **36**, 1373 (2009).
34. P. de Gennes and J. Prost, *The Physics of Liquid Crystals*, 2nd ed., Clarendon Press Oxford (1993).
35. A. Yariv, *Optical Electronics in Modern Communications*, 5th ed. Oxford University Press, New York, (1997).

Biographies and photographs of the authors are not available.